# Grating-based Tomography of Human Tissues

Bert Müller[a], Georg Schulz[a], Andrea Mehlin[a], Julia Herzen[b,c], Sabrina Lang[a], Margaret Holme[a], Irene Zanette[c,d], Simone Hieber[a], Hans Deyhle[a], Felix Beckmann[b], Franz Pfeiffer[c] and Timm Weitkamp[d,e]

[a]*Biomaterials Science Center, University of Basel, Switzerland*
[b]*Institute of Materials Research, Helmholtz-Zentrum Geesthacht, Germany*
[c]*Physics Department, Munich University of Technology, Germany*
[d]*European Synchrotron Radiation Facility, Grenoble, France*
[e]*Synchrotron Soleil, Gif sur Yvette, France*

**Abstract.** The development of therapies to improve our health requires a detailed knowledge on the anatomy of soft tissues from the human body down to the cellular level. Grating-based phase contrast micro computed tomography using synchrotron radiation provides a sensitivity, which allows visualizing micrometer size anatomical features in soft tissue without applying any contrast agent. We show phase contrast tomography data of human brain, tumor vessels and constricted arteries from the beamline ID 19 (ESRF) and urethral tissue from the beamline W 2 (HASYLAB/DESY) with micrometer resolution. Here, we demonstrate that anatomical features can be identified within brain tissue as well known from histology. Using human urethral tissue, the application of two photon energies is compared. Tumor vessels thicker than 20 µm can be perfectly segmented. The morphology of coronary arteries can be better extracted in formalin than after paraffin embedding.

**Keywords:** Thalamus, urethra, tumor vessels, plaque, synchrotron radiation, phase tomography.
**PACS:** 68.37.Yz; 87.57.Q-; 87.85.Pq.

## INTRODUCTION

The main health problems in our aging society relate to atherosclerosis, cancer, musculoskeletal system, and degenerative diseases of the brain. While the hard tissues have been successfully visualized by means of hard X-ray tomography in the conventional absorption contrast mode, the anatomical features in soft tissues such as brain and urethra as well as tumors and vessels only provide limited differences in X-ray absorption, because they predominately consist of water and light elements. Phase tomography, however, yields such a high contrast that many microstructures become visible even if staining procedures are avoided [1-3]. The spatial resolution of grating-based phase tomography, however, does not yet reach the lateral spatial resolution of the well-established histology. Therefore, it is worth comparing two-dimensional histological sections of the brain with the less detailed but three-dimensional phase tomography data obtained before sectioning. Furthermore, the imaging parameters such as the selected photon energy have to be optimized. For example, one may compare the phase tomography data of a human urethra acquired at two photon energies keeping the overall system unchanged, i.e. just to use two Talbot orders.

*International Workshop on X-ray and Neutron Phase Imaging with Gratings*
AIP Conf. Proc. 1466, 107-112 (2012); doi: 10.1063/1.4742277

## MATERIALS AND METHODS

### Urethral Tissue Preparation and Imaging

A urethra from a 65-year-old woman was post mortem removed at the Department of Legal Medicine at the University Hospital in Hamburg-Eppendorf, Germany. The region of the urethra next to the bladder neck was selected for imaging as at this position an artificial urinary sphincter is placed in patients, who suffer from severe urinary incontinence. The tissue embedded in formalin was transferred in a cylindrical polymer container 2 cm in diameter. During the measurements the container was placed in a 3 and 2.5 cm-wide, rectangular water reservoir, respectively.

The measurements at the beamline W 2 (HASYLAB at DESY, Hamburg, Germany) operated by the Helmholtz-Zentrum Geesthacht, Germany were performed using photon energies of 22 keV and 31 keV, respectively. These photon energies correspond to the seventh and the fifth Talbot order (details see ref. [4]). The three-dimensional imaging data were obtained from 1'000 projections each with a pixel size of about 14 μm.

### Brain Tissue Preparation and Imaging

The brain was extracted from a donated male body at the Institute of Anatomy (University of Basel, Switzerland) and subsequently transferred to formalin solution for fixation. After two weeks of fixation, a block of the thalamus about $3 \times 3 \times 3$ cm$^3$ in size was extracted at the Neurosurgery Department (University Hospital Zurich, Switzerland) and placed in a polymer container filled with 4% formalin solution.

The grating interferometry experiment was carried out at the beamline ID 19 (ESRF, Grenoble, France).[5, 6] The photon energy of 26 keV, the beam splitter grating with a periodicity of 3.99 μm, the analyzer grating with a periodicity of 2 μm (both fabricated at the Paul Scherrer Institut (Villigen, Switzerland) were arranged to measure at the ninth Talbot order. The container with the thalamus in formalin solution was suspended from a rotation stage and immersed in a water tank. The effective pixel size corresponded to 30 μm. As the specimen width was larger than the field of view, the experiment was performed with an asymmetric axis position, shifted by 9 mm from the center of the detection unit (see e.g. ref. [7]). Projection radiographs were taken in 799 steps over a range of 360°. At each projection angle, a phase-stepping scan of four steps over one fringe period was taken.[8] The projection dataset was reconstructed using a modified filter kernel in combination with standard filtered back-projection algorithm.

After the SRμCT experiments, the block was transferred in progressively increasing sucrose concentrations over around two weeks for cryo-protection. The block was then frozen by immersion in isopentane (-30 °C) and stored at a temperature of -75 °C. Using a Leica CM 3050, cryostat sections, 50 μm thick, were collected in 0.1 M phosphate buffer. For the staining procedure, the sections were mounted on gelatinized slides and stained for Nissl with cresyl violet. The sections were then recorded (HP

scanjet 7400c). Microphotographs of selected thalamic areas were taken using a Leica MZ16 microscope and DFC420-C digital camera.

## Human Coronary Artery Preparation and Imaging

A constricted human coronary artery was measured twice at beamline ID 19, once in formaldehyde and subsequently after embedding in paraffin (beam-splitter pitch: 4.8 μm; pitch of analyzer: 2.4 μm). A photon energy of 53 keV was selected. The distance between the gratings was 370 mm (3$^{rd}$ Talbot order). The detector, with 2048 × 2048 pixels and an effective pixel size of 7.5 μm, was placed about 10.5 cm downstream of the analyzer grating. Projection radiographs were taken over a range of 360° in step sizes of 0.36036°. At each projection angle, four phase-stepping images were taken. The exposure time for each image was 2 s. The reconstruction procedure was the same as for the brain tissue.

## Tumor Specimen Preparation and Imaging

C51 tumor cells were injected into nude mice to grow tumors in strict adherence to the Swiss law from animal protection. Immediately after extraction the tumor 3 mm in diameter was fixed in 5% para-formaldehyde. For the tomography experiment, the tumor was placed in a polymer tube. The CCD-based digital detector at ESRF-ID19 had an effective pixel size of 3 μm after two-fold binning. The grating periods were 4 μm (beam splitter) and 2 μm (analyzer) for a photon energy of 17.6 keV. The fifth Talbot order was used, i.e., the gratings were separated by 140 mm. The exposure time for the 359 projections along 360° was set to 0.3 s for each detector frame

# RESULTS AND DISCUSSION

Figure 1 compares the histological slice with the related virtual one from phase tomography. The Nissl stain using cresyl violet allows differentiating between grey nuclei on the basis of cyto-architectonic characteristics in terms of cell sizes and densities. Here, the cells adopt a blue color. The experts in brain anatomy can identify numerous features including the anteroventral nucleus (AV), the thalamic nucleus (R), the internal capsule (ic), the putamen (PuT), the mediodorsal nucleus (MD), the ventral lateral nucleus (VL), the ventral anterior nucleus (VA), the zona incerta (ZI), the subthalamic nucleus (STh), the globus pallidus, internal (GPi) and external (GPe) segments as well as the optic tract (ot). Most of these characteristic features can also be detected in the phase tomography slice without the application of any staining protocol. Therefore, preparation artifacts including local shrinkage caused e.g. by cutting and staining were avoided. The 3D micro-architecture of the anisotropic and heterogeneous brain tissue with isotropic spatial resolution can be further evaluated.

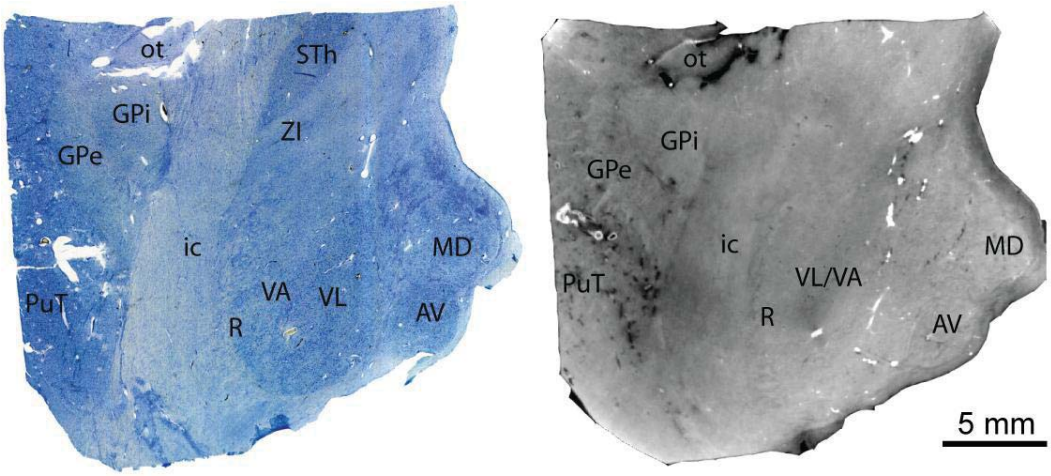


**FIGURE 1.** Virtual slices from phase tomography data allow assessing the microstructures in human brain in a similar fashion as known from currently used, state-of-the-art histology. The abbreviations are explained in the text.

The human urethra was measured at two photon energies. Therefore, the results obtained from two Talbot orders can be compared. Figure 2 shows the registered 3D data[9] by three virtual cuts orthogonal to each other. The main anatomical features can be recognized including the lumen filled with formalin in the center. In the histograms below the electron density relative to water $\Delta\rho$ is plotted. The components with a higher density are smaller than zero and the ones with a lower density larger. The highest peak corresponds to the parts of the urethral tissue with weak structure (tunica mucosa). The peak in the center of the histogram arises from formalin solution. The broad peak at the right (positive $\Delta\rho$ values) corresponds to the (bright) fatty tissue and the container. Note, the peaks are not directly comparable but significantly shifted for the two photon energies/Talbot orders although the electron density is regarded as energy independent. The reason for the shifted $\Delta\rho$ values could lie in the vertical gradient of the photon energy at the beamline. As expected, the sensitivity (see full-width-of-half-maximum of the peaks or the overlap of the formalin and the tissue peak of the scan at 31 keV) is much higher for the measurement at 22 keV. This measurement, however, was much more time consuming (31 h instead of 11 h for the measurement at 31 keV), which is mainly due to the photon flux ratio resulting in an exposure time longer by one order of magnitude. For the quantitative comparison of the data sets measured at the two photon energies factors including visibility much higher for the scan at 21 keV and the sensitivity have to be taken into account.

Figure 3 compares slices of plaque-containing arteries in formalin (left) and after embedding in paraffin (right). In both images the artery walls, plaque and surrounding fatty tissue are clearly visible. The shape of the specimen is only slightly affected by the embedding procedure. From the comparable slices, however, it appears that formalin is a more suitable medium for imaging non-decalcified human coronary arteries in phase tomography.

Figure 4 shows the segmented vessel tree of the tumor tissue. The vessels thicker than about 20 µm are well represented although the spatial resolution derived from contrast-to-noise ratio was not better than 60 µm. Vessels with diameters below 20 µm appear spotted. The smallest capillaries having diameters of about 4 µm cannot be

detected using the presently available grating tomography systems. Therefore, the improvement of the spatial resolution is an important task.

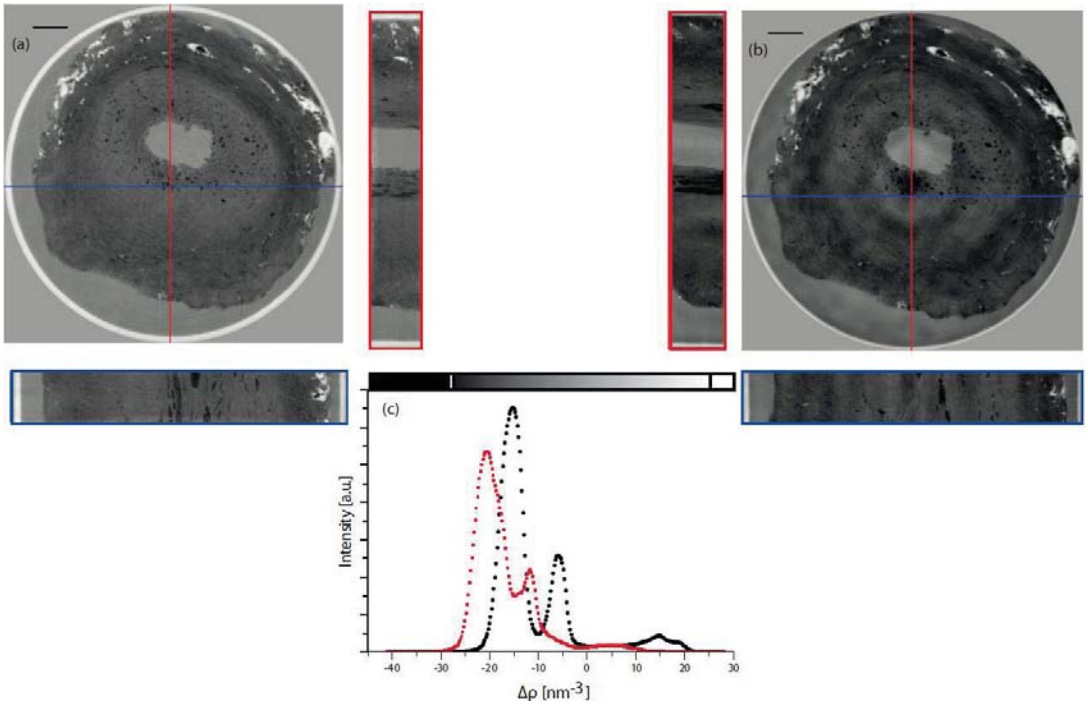


**FIGURE 2.** (a) Reconstructed slice of the phase tomogram acquired with 22 keV photons together with perpendicular cuts; (b) Corresponding data recorded at 31 keV (c) At first glance, the histograms of the electron densities show the quantitative differences (black - 22 keV and red - 31 keV). Appropriate corrections are necessary. The scale bars correspond to 2 mm.

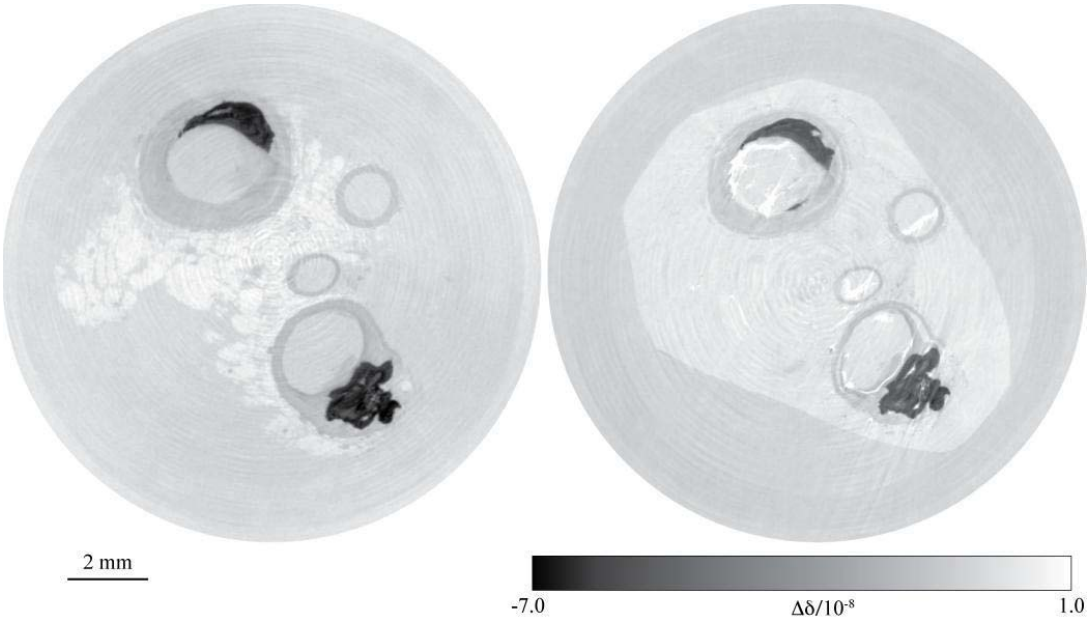


**FIGURE 3.** Axial slices of a non-decalcified human coronary artery measured in phase contrast SRμCT in formalin (left) and after embedding in paraffin (right).

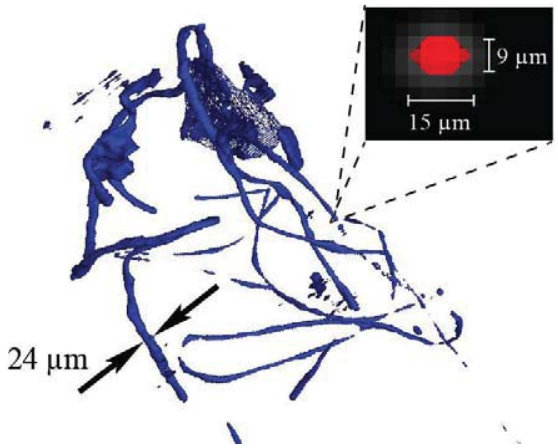


**FIGURE 4.** Tumor vessels with diameters larger than 20 µm can be segmented easily, whereas thinner vessels appear spotted. In order to visualize the smallest capillaries, the spatial resolution would have to be improved by a factor of two.

## ACKNOWLEDGMENTS

The authors thank Magdalena Müller-Gerbl (University of Basel), Klaus Püschel (University of Hamburg), and Marco Dominietto (ETH Zürich) for tissue preparation. The financial support of the Swiss National Science Foundation (grants CR2312_125406/1 and 200021 127297/1) is gratefully acknowledged. Beamtime was kindly provided by HASYLAB/DESY (II-20060035 EC) and ESRF (MD-328, MD-498, MI-983). T.W. acknowledges support from the French research networks RTRA *Digiteo* and *Triangle de la Physique* (grants 2009-034T and 2009-79D).

## REFERENCES

1. F. Pfeiffer, O. Bunk, C. David, M. Bech, G. Le Duc, A. Bravin and P. Cloetens, Phys. Med. Biol. **52**, 6923-6930 (2007).
2. G. Schulz, T. Weitkamp, I. Zanette, F. Pfeiffer, F. Beckmann, C. David, S. Rutishauser, E. Reznikova and B. Müller, J. Roy. Soc. Interface **53** (7), 1665-1676 (2010).
3. T. Weitkamp, C. David, O. Bunk, J. Bruder, P. Cloetens and F. Pfeiffer, Eur. J. Radiol. **68**, S13-S17 (2008).
4. J. Herzen, T. Donath, F. Beckmann, M. Ogurreck, C. David, J. Mohr, F. Pfeiffer and A. Schreyer, Rev. Sci. Instrum. **82**, 113711 (2011).
5. T. Weitkamp, P. Tafforeau, E. Boller, P. Cloetens, J.-P. Valade, P. Bernard, F. Peyrin, W. Ludwig, L. Helfen and J. Baruchel, AIP Conf. Proc. **1221**, 33-38 (2010).
6. T. Weitkamp, I. Zanette, C. David, J. Baruchel, P. Bernard, M. Bech, H. Deyhle, T. Donath, J. Kenntner, S. Lang, J. Mohr, B. Müller, F. Pfeiffer, E. Reznikova, S. Rutishauser, G. T. Schulz, A. and J.-P. Valade, Proc. SPIE **7804**, 780406 (2010).
7. B. Müller, R. Bernhardt, T. Weitkamp, F. Beckmann, R. Bräuer, U. Schurigt, A. Schrott-Fischer, R. Glueckert, M. Ney, T. Beleites, C. Jolly and D. Scharnweber, Int. J. Mat. Res. **98** (7), 613-621 (2007).
8. T. Weitkamp, A. Diaz, C. David, F. Pfeiffer, M. Stampanoni, P. Cloetens and E. Ziegler, Optics Express **13** (16), 6296-6304 (2005).
9. B. Müller, H. Deyhle, S. Lang, G. Schulz, T. Bormann, F. C. Fierz and S. Hieber, Int. J. Mater. Res. **103** (2), 242-249 (2012).